Infrared study of hydrogen chemisorbed on W(100) by surface-electromagnetic-wave spectroscopy

Y. J. Chabal* and A. J. Sievers
Laboratory of Atomic and Solid State Physics, Cornell University, Ithaca, New York 14853
and Materials Science Center, Cornell University, Ithaca, New York 14853
(Received 3 March 1981)

The ν_1 vibrational mode of H chemisorbed on W(100) at saturation coverage has been measured at high resolution by infrared surface-electromagnetic-wave (SEW) spectroscopy. This technique is observed to provide an order-of-magnitude larger contrast ratio for weak vibrational modes on metal surfaces than is expected from reflection-absorption spectroscopy. A UHV compatible geometry has been devised so that SEW's can be excited on the W(100) surface with a quasitunable CO_2 laser. We find that at room temperature the center frequency and absorption strength of the ν_1 mode, as measured with SEW's, are in good agreement with electron-energy-loss-spectroscopy measurements. In addition, our high-resolution study leads us to postulate that the ν_1 absorption is composed of a sharp zero-phonon line surrounded by broad one-photon sidebands.

I. INTRODUCTION

Because of its intrinsic high-spectral-resolution capability,[1] infrared spectroscopy was one of the first techniques used for the study of vibrational modes of adsorbates on metal surfaces.[2] Unfortunately, reflection-absorption (RA) spectroscopy is very insensitive to the small dipole moments associated with vibrational modes on metal surfaces; so far the technique has been limited to the study of strong internal modes of the adsorbate such as CO on various metal substrates.[3-8] In addition, the strong electromagnetic selection rules at metal surfaces limit the infrared (ir) studies to those modes in which the vibrational motions are perpendicular to the surface.[2-9]

In the past few years the most progress in the field of vibrational spectroscopy of adsorbates on metal surfaces has been made with electron energy-loss spectroscopy (EELS).[10-14] Its high sensitivity to low adsorbate coverages, its broad-band capabilities (100–3000 cm^{-1}) and, as recently shown,[14] its ability to detect vibrational modes parallel to the surface by off-specular reflection make it an invaluable technique for a multitude of surface studies, particularly for the identification of surface complexes (chemistry) and surface sites (geometry). However, the low resolution of EELS (>40 cm^{-1}) limits its usefulness for the accurate study of the spectral shapes of vibrational modes. For example, the internal vibrational modes of CO on Pd(100) (Ref. 15) and Ru(100) (Ref. 16) exhibit subtle variations in spectral width and shape as a function of coverage and temperature on an energy scale of a few cm^{-1}.

The H/W(100) system has been studied by a variety of techniques, such as low-energy electron diffraction (LEED),[17-19] Rutherford backscattering spectroscopy (RBS),[20] and EELS,[12-14] which have contributed to the establishment of a consistent static model. In this model the H atom is chemisorbed on a bridge site both for low and high coverage; however, for high coverage (saturation coverage) the hydrogen forces the W surface back into registry with the bulk atoms.[12-14,17-20] The vibrational frequency associated with the ν_1 mode ($H-W_2$ symmetric stretching mode perpendicular to the surface) shifts accordingly as the surface W atoms move back in registry with the bulk as shown by EELS.[12-14] Puzzling features in the EELS spectrum regarding the linewidth of this ν_1 mode remain unexplained: For low-H coverage, the EELS measures a 60-cm^{-1}-wide line while at high coverage, a 120-cm^{-1}-wide line is resolved. Such a wide line ($\Delta\omega/\omega_0 \cong 0.1$) is surprising since the H atoms have a unique and well-defined absorption site (bridge site) on the reconstructed W surface atoms. It is the physical processes behind this broad line that we intend to explore by high-resolution spectroscopy.

In the past decade a number of studies of ultrathin dielectric films on metal surfaces have been made with a new ir probe, surface-electromagnetic-wave spectroscopy (SEW).[21,22] So far this technique, which appears to be simpler than ir ellipsometry and more sensitive than RA spectroscopy, has only been applied to samples under ambient conditions.[23]

In this paper we first show that SEW spectroscopy can be adapted to UHV conditions and then use this high-resolution probe to study the ν_1 vibrational mode of hydrogen chemisorbed on W(100) for a saturation coverage. With the order-of-magnitude increase in contrast ratio provided by SEW compared to RA spectroscopy, we

measure an absorption line whose center frequency is in good agreement with earlier EELS measurements[12-14]; however, the SEW-measured linewidth (14 cm^{-1}) is much smaller than the EELS-measured linewidth (120 cm^{-1}). Since the SEW measurement (with increased sensitivity) should measure the same spectrum as the EELS measurement (with increased resolution) the different linewidth results indicate that the ν_1 band must contain fine structure. A model in which the structure consists of a zero-phonon line and its associated one-photon sidebands explains the available data.[24]

In the next section we compare the RA and SEW spectroscopies and provide the motivation for choosing SEW's. We then show how the SEW probe is made compatible with UHV requirements. The spectroscopic data for H on W(100) are presented and various experimental errors are discussed. In Sec. III, we compare our data with the EELS results, and show that both sets of data are consistent with a model wherein the ν_1 vibrational mode strongly interacts with the W phonons. Finally, in Sec. IV, we propose a number of tests of the model.

II. EXPERIMENTAL

A. Comparison of RA and SEW spectroscopies

A number of investigators have proposed that surface electromagnetic waves (SEW's) can be used to probe the vibrational spectra of molecules adsorbed on metal surfaces.[23] These bound TM modes have an evanescent field distribution on both the metal and the vacuum sides of the interface with the maximum E field at the boundary and perpendicular to it. In the infrared (10 μm wavelength), SEW's have a propagation length of 1 cm.[25] To date, there has been only one direct comparison of SEW and RA spectroscopies,[26] so we begin with the argument which led us to choose one technique over the other. The adsorbate is modeled by a layer of optical thickness d and absorptivity A.

For RA spectroscopy with a weak source so that the measurement is detector noise limited, Greenler[27] showed that the signal-to-noise ratio is optimized for the TM polarization when ΔR (the depth of an RA band) is maximized with respect to the number of reflections N_0. This maximum value occurs when

$$(R_0)^{N_0} = e^{-1}, \tag{1}$$

where R^0 is the reflection coefficient associated with one reflection for a particular angle of incidence (typically $\approx 85°$).

For large angles of incidence ($45° \leq \theta \leq 86°$), the fractional change in reflectivity for N_0 reflections is[28]

$$\frac{\Delta R}{R}(\theta) \approx N_0 A \frac{\sin^2\theta}{\cos\theta} . \tag{2}$$

The $\sin^2\theta$ factor occurs because only the component of the E field perpendicular to the surface is important. The angular dependence of the optical path gives the $\cos\theta$.

For SEW spectroscopy with an incident beam intensity I_0, the intensity detected at the detector is

$$I = C^2 I_0 \exp(-\alpha l) , \tag{3}$$

where C^2 is the product of the input and output coupling efficiencies onto and off of the metal surface and l is the length of the surface probed. The absorption coefficient $\alpha_t = \alpha_m + \alpha_a$, where α_m is due to the metal and α_a is due to the adsorbate. The adsorbate-induced change in the transmitted intensity across the surface ΔI due to the presence of α_a is[29]

$$\Delta I = C^2 I_0 \exp(-\alpha_m l)[1 - \exp(-\alpha_a l)] . \tag{4}$$

Differentiating ΔI with respect to l gives the optimum probing length l_0, for which ΔI is a maximum, namely,

$$l_0 = -\frac{1}{\alpha_a} \ln\left(1 - \frac{\alpha_a}{\alpha_a + \alpha_m}\right) . \tag{5}$$

The fraction absorbed is

$$\frac{\Delta I}{I} = 1 - \exp(-\alpha_a l_0) = \frac{\alpha_a}{\alpha_a + \alpha_m} . \tag{6}$$

Since $\alpha_a \ll \alpha_m$ for one monolayer or less, then

$$l_0 \approx \alpha_m^{-1} \tag{7}$$

and

$$\frac{\Delta I}{I} \approx \frac{\alpha_a}{\alpha_m} \approx \alpha_a l_0 \equiv A_{\mathrm{SEW}} . \tag{8}$$

We now must relate the A_{SEW} for evanescent waves to the A obtained for plane waves. Because much of the SEW wave is spatially removed from the adsorbate layer, A_{SEW} is smaller than A by the factor d/δ, where δ is the extent of the SEW into the vacuum[23]; however, since the SEW interacts over the length l_0 instead of the thickness d, $A(d/\delta)$ is increased by the additional factor (l_0/d). The resultant expression is

$$A_{\mathrm{SEW}} = A\left(\frac{l_0}{\delta}\right) . \tag{9}$$

Combining Eqs. (2), (8), and (9), we obtain

$$\frac{\Delta I}{I} \approx \frac{l_0}{\delta} \frac{\cos\theta}{N_0 \sin^2\theta} \frac{\Delta R}{R} . \tag{10}$$

For a Drude metal substrate[21] with $\omega\tau > 1$:

$$\alpha_m \cong \left(\frac{\omega}{\omega_p}\right)^2 \frac{1}{c\tau} , \tag{11}$$

$$\delta = \frac{c\omega_p}{2\omega^2} , \tag{12}$$

and a weak absorber, such that $\alpha_a \ll \alpha_m$, then one has

$$l_0/\delta \cong (\alpha_m \delta)^{-1} \approx 2\omega_p \tau , \tag{13}$$

where ω_p and τ are the metal plasma frequency and the electron relaxation time, respectively. Inserting Eq. (13) into Eq. (10) we obtain the desired relation, namely,

$$\frac{\Delta I}{I} = (2\omega_p \tau)\left(\frac{\cos\theta}{N_0 \sin^2\theta}\right)\frac{\Delta R}{R} . \tag{14}$$

Let us put some typical numbers into this expression. For $\theta = 85°$ and $N_0 = 2$, $\cos\theta/\sin^2\theta \sim 10^{-1}$ and for most metals $\omega_p\tau \sim 10^2$, so that $\Delta I/I$ is an order of magnitude larger than $\Delta R/R$. Given equal probing intensity at the metal-adsorbate interface, SEW spectroscopy would provide more sensitivity in the detector noise-limited regime. However, because of the low-coupling efficiency [for the edge coupler $C^2 \sim 10^{-2}$ in Eq. (3)], little improvement can be expected over RA spectroscopy if a very weak source is used.

However, if one makes measurements with a strong ir laser source then it is the source noise, not the detector noise, which dominates and a different comparison of the two spectroscopies should be made. Because source noise is proportional to the intensity the signal-to-noise ratio is optimized by maximizing the contrast, namely, $\Delta R/R$ or $\Delta I/I$. Although both Eq. (2) (for $\Delta R/R$) and Eq. (8) (for $\Delta I/I$) indicate that the sample should be made as long as possible in the strong source limit, one can compare the two techniques by requiring that the two contrasts be equal, therefore,

$$\frac{\Delta R_N}{R_N} = \frac{\Delta I}{I} . \tag{15}$$

The subscript N refers to the number of reflections needed in RA spectroscopy to satisfy Eq. (14), namely,

$$N = 2\omega_p \tau \frac{\cos\theta}{\sin^2\theta} . \tag{16}$$

For W, $\omega_p\tau = 140$ and $\theta = 85°$, then $N = 25$ reflections. For the RA measurement, the increase in sample length should be about 10 to 50 times, and the decrease in signal throughput about 10^{-3} times the corresponding values for the SEW measurement. Since the sample length for SEW measurements in the 10-μm region are of the order of 1 cm, the corresponding RA samples are impractical. We conclude that in the strong-source limit SEW spectroscopy is to be preferred in the ir.

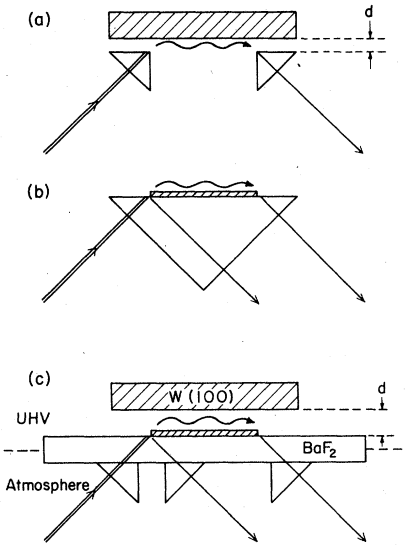

FIG. 1. Different geometries for exciting SEW's on metal surfaces (a) The two-prism coupling geometry. The coupling efficiency depends on the gap d. (b) The edge coupler geometry. The SEW's are excited on the top face of the evaporated metal film. The reflected beam is well separated from the transmitted SEW beam. (c) The hybrid geometry used for UHV studies. The sensitivity of SEW to the W(100) surface depends on the gap d. The reflected beam is well separated from the transmitted SEW beam.

B. Apparatus

The fundamental experimental problems associated with SEW spectroscopy stem from the strict requirement, both in frequency and angular profile, imposed on the incident radiation for efficient excitation of SEW's on the metal. The coupling geometry which we decided on is shown in Fig. 1(c). It combines features of both the two-prism coupler used by earlier workers, which is shown in Fig. 1(a), and the edge coupler which is shown in Fig. 1(b). Making this configuration compatible with UHV requirements has produced an unusual UHV chamber and optical layout.

1. UHV chamber

The UHV chamber consists of a "T" with 6 ports and is pumped by both a 220-liter-triode ion pump and a titanium sublimation pump with a liquid N_2 shroud. A gate valve separates the system from the ion pump so that the chamber can be pumped

only by the cold sublimator during H_2 exposure, thus reducing the CO contamination. The working base pressure is 1.5×10^{-10} Torr with H_2, He, and CH_4 as principal contaminants, as detected by a Leybold-Heraeus-Quadruvac 200-mass spectrometer equipped with an electron multiplier head.

The sample manipulator is a Huntington linear-motion feedthrough with an 8-in. stroke and is mounted horizontally in the 6-in. port facing the window assembly. It is based on a micrometer screw mechanical design with a resolution of 25 μm, bellows sealed and mounted on a $2\frac{3}{4}$-in. flange. An adaptor flange, which goes from this $2\frac{3}{4}$-in. flange to the 6-in. side port of the chamber, is equipped with eight electrical feedthroughs and two liquid N_2 feedthroughs. The sample holder is a stainless-steel liquid N_2 reservoir as shown in Fig. 2. The electrical connections are made with tungsten rods insulated from the chamber by quartz tubes and connected to the electrical feedthroughs by means of sliding contacts. The W(100) sample is held by two tungsten rods resting on sapphire insulators. A thoriated W filament is mounted at about $\frac{1}{4}$ in. behind the sample. A tungsten shield prevents electrons from hitting the rest of the holder.

A $2\frac{1}{4}$-in.-diameter BaF_2 window is sealed to a thin silver insert by means of a bakeable and low-vapor-pressure silicone resin (Vacseal) as a bonding material. The silver insert is welded to the $4\frac{1}{2}$-in. conflat flange as shown in Fig. 2. Since silver and barium fluoride have almost the same coefficient of thermal expansion in the range -100 to $+100$ °C, this seal has withstood a large number of thermal cyclings.[30]

2. Optics

The ir source is a 20-W tunable CO_2 laser. By aperturing the laser cavity a near Gaussian beam with good spatial stability is obtained. Although this modification cuts the output power to a few tenths of a watt and suppresses weak laser lines, the relative strengths of the remaining lines are evened out. The source is line tunable from 925 to 955, 970 to 985, 1037 to 1054, and 1070 to 1082 cm^{-1} with a line every 1.5 to 2 cm^{-1}.

The optical layout is illustrated in Fig. 3(a). A polarized CO_2 beam chopped at a frequency f_1 passes through an adjustable polarization rotator (WP), a long-focal-length lens (L_1), and a KCl beam splitter (BS), and is then focused on the edge of the gold film (1.3×0.4 cm^2) evaporated on the vacuum side of the window. The coupling of the SEW to the crystal is shown in Fig. 3(b) and will be discussed shortly. The total internal reflected beam from the vacuum-window interface is eliminated from the detecting system by a shield (S).

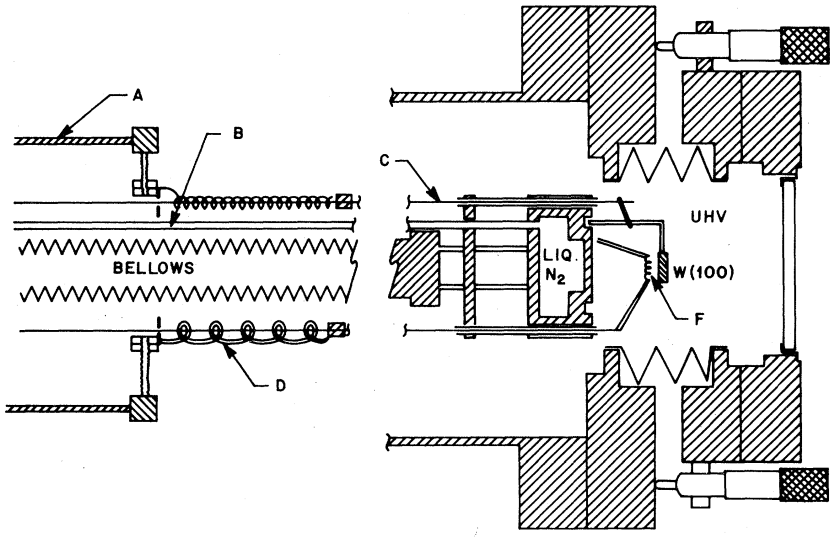

FIG. 2. Detail of the manipulator and window-port assembly. Note the sliding contacts on the left, the sample holder with a liquid N_2 reservoir, the sample which is spotwelded to W rods, and the BaF_2 window mounted on a movable port. The W rods labeled C provide contact to the sample, to the filament F, and to thermocouple leads. These rods are electrically connected to the copper feedthroughs A, by a copper braid D or stainless-steel springs (depending on the current requirement) so that they may be translated, B is the liquid-nitrogen fill line.

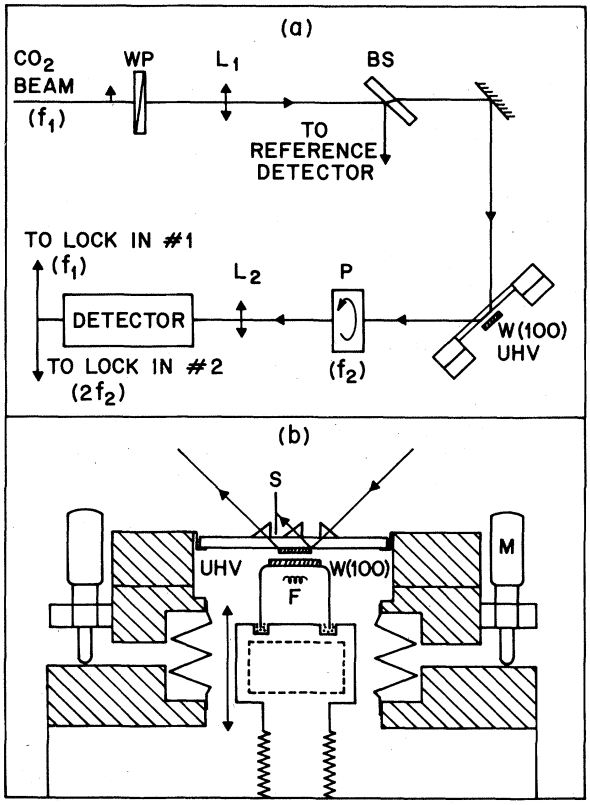

FIG. 3. (a) Schematic drawing of the infrared optics. The CO_2 beam is chopped at f_1 and is polarized. WP is a zero-order waveplate allowing the polarization to be rotated. L_1 is a 15-in. lens, BS is a 1-cm-thick KCl beam splitter sending part of the beam to a reference detector, while the transmitted beam continues to the window. P is a polarizer rotating at a frequency f_2. L_2 is a 2.5-in. lens. (b) Schematic drawing of the window assembly and sample holder. Note the shield S preventing the reflected beam from interfering with the transmitted SEW beam. F is a thoriated W filament for electron bombardment of the sample. The double-headed arrow indicates that the sample holder can be translated forward and backward with respect to the window. M is one of the four micrometers.

After probing 1.3 cm of the W(100) surface, the SEW is decoupled and passes through a polarizer (P) rotating at frequency f_2 before being focused by a short-focal-length lens (L_2) onto a pyroelectric detector, as shown in Fig. 3(a). The measurements consist of determining both the change in SEW transmission ΔI and the transmission I. In order to eliminate both the laser-intensity fluctuations and spatial drifts (affecting the coupling), and to enhance the ΔI measurement, we used a double-beam geometry. When the W crystal is close to the gold film, we rotate the incoming polarization from a purely TM-polarized beam to a mixture of TM and TE so that TE waveguide modes are also launched between the gold and the tungsten, in addition to the TM-SEW mode. Some of this TE radiation is scattered at the gold-film output edge through the polarizer (P) to the detector. By adjusting the polarization angle, the TE signal, which does not interact with the chemisorbed hydrogen, can be made the same size as the TM-SEW signal, which does interact. The output of lock in 2, tuned at $2f_2$, is thus nulled and the sensitivity to small ΔI is increased. Lock in 1, tuned at f_1, records $\frac{1}{2}(I_{TM}+I_{TE})=I_{TM}$ since the two intensities are balanced.

C. Sample details

1. Preparation

The W(100) ingots were oriented, spark cut, and polished. Several different sizes were used. The thin crystals (0.2 cm) had e^- beam welded W rods as support, while the thicker ones could simply be spot welded to W rods.

The sample cleaning procedure consisted of 30-min periods of electron bombardment heating of the sample at 1200 °C in about 8×10^{-8} Torr O_2, separated by flashes at 2000 K at a pressure of 3×10^{-10} Torr. The typical integrated baking time in O_2 was 6 to 10 h. Although our system was not equipped with an Auger system, the above procedure was judged more than adequate by Wojcik *et al.*,[31] who used tungsten crystals from the same boule and determined the cleanness of the surface with Auger. Our criterion of sample cleanness was to obtain reproducible flash-desorption spectra with well-defined strength for both O_2 and H_2 adatoms at saturation coverage.

2. Surface sensitivity

The critical parameter for an SEW transmission measurement is the gap d between the W(100) crystal and the gold film, as shown in Fig. 1(c). To establish an experimental guide for the UHV experiments, the gap dependence of the surface sensitivity has been obtained from an independent measurement outside the vacuum system. A W(100) crystal (about 1.5-cm long) was coated with about 70 Å of $KReO_4$, a dielectric which is known[32] to have a vibrational mode near 10.6 μm, and placed next to an edge coupler unit with a 1.2-cm-long Au film. The schematic arrangement is shown in the lower left corner of Fig. 4(a). Mylar spacers were used to vary the gap d, and the throughput and frequency-dependent transmission was measured as a function of this gap. The percent transmission is plotted versus

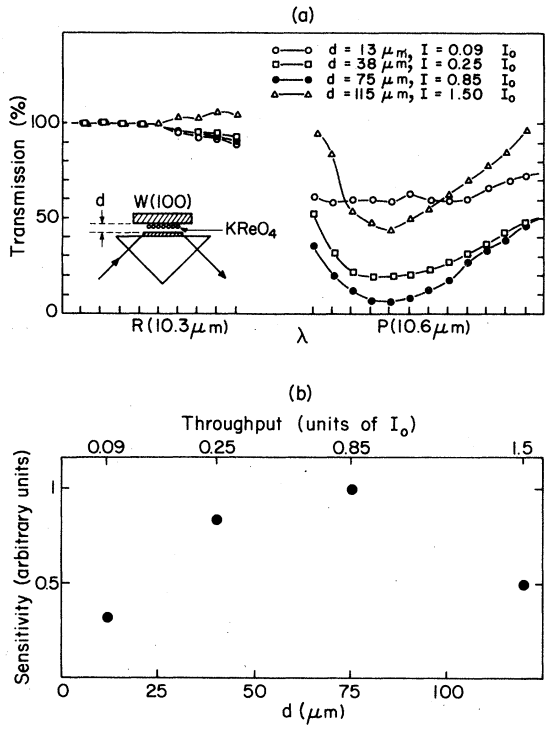

FIG. 4. (a) Transmission curves for the system shown at the bottom left corner as a function of frequency for several gap values. (b) Plot of the effective sensitivity obtained from the above transmission plot.

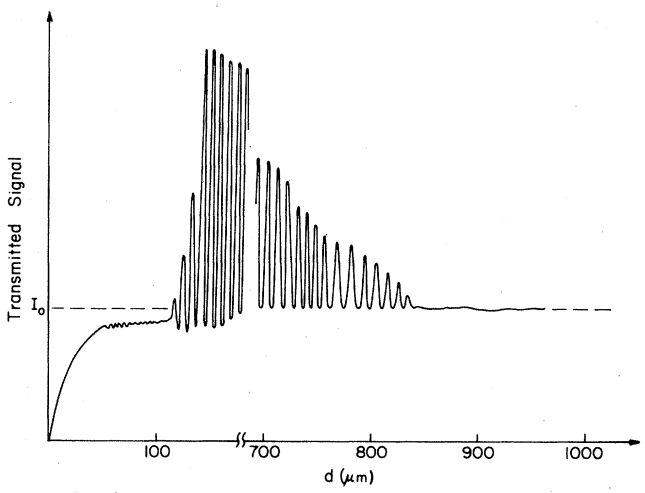

FIG. 5. Schematic drawing of the transmitted signal versus gap as the W(100) crystal is brought close to the gold film. Note the discontinuous scale.

frequency in Fig. 4(a) and the effective sensitivity, is plotted versus gap in Fig. 4(b). Several points should be noted as follows:

(a) Since the dispersion of BaF_2 is quite large at 10.6 μm, the critical angle increases substantially with increasing wavelength. At long wavelengths more intensity is refracted into the vacuum and couples to waveguide modes with $k_x \lesssim (\omega/c)$. At small gap settings this effect is less pronounced since a smaller fraction of the intensity is converted to waveguide modes.

(b) The optimum sensitivity occurs for $d \approx 75$ μm, where the throughput is about 0.85 of the pure SEW transmitted intensity, i.e., in the limit of a very large gap.

(c) When the optimum gap of 75 μm is used, the W surface is probed with the same surface sensitivity as obtained in the single-surface geometry shown in Fig. 1(b).

Figure 5 shows an approximate representation of the transmitted signal as a function of the gap when the W(100) is brought close *inside* the vacuum system. I_0 is the pure SEW transmitted signal obtained when the W crystal is far away. Complicated waveguide mode patterns take place but the region around 75 μm can usually be recognized. The dependence of the transmitted signal on the gap was the easiest way to estimate the *average* gap distance.

3. *Sample alignment*

Two techniques were used to align the window parallel to the W(100) surface at the beginning of a series of runs. (a) The back reflection of an He-Ne laser was monitored 20 in. away from the window. The reflection from the window produced a faint spot which could be compared with the stronger spot from the W crystal, which was wider and longer than the gold film. By adjusting the window micrometers, the relative alignment could be modified accurately. (b) To determine which part of the W sample was touching the gold film an electrical scheme was devised using an array of thermocouples as shown in Fig. 6(a). The sample was electrically isolated from the chamber ground. By monitoring the resistance between the sample and the ground, one could determine when the crystal touched one of the gold pads. Next, by monitoring the voltage between the sample and the ground, as shown in Fig. 6(b), and by illuminating each chromium pad with a microscope lamp, one can determine which gold pad is in contact with the sample. The Ni-Au thermocouple junction gave a 3-μV voltage rise when illuminated. For instance, in the example shown in Fig. 6(b), only junction 3 will give a reading when illuminated. This technique proved very useful in the early stages of alignment of a new sample whose surface was not particularly

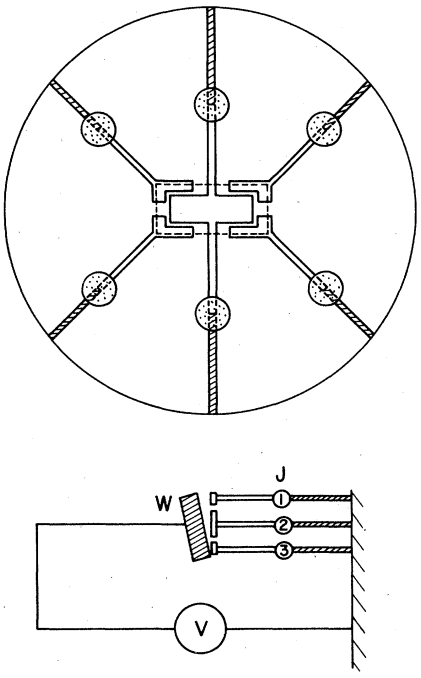

FIG. 6. (a) Drawing of the thermocouple array for window positioning. The clear areas are gold, the hatched areas are nickel, and the dotted areas are chromium. (b) Schematic representation of the electrical circuit associated with the thermocouples.

flat at the edges, making the optical alignment difficult.

If the sample is well aligned so that the ν_1 absorption line can be seen, a check on the average gap value can be obtained by measuring the time it takes to obtain a saturation coverage of H for a given exposure pressure (usually 4×10^{-8} Torr) when the W sample is in position. For a sample of length l and width w positioned at a distance d from the window, the effective area through which the H_2 molecules must pass in order to be adsorbed is $2d(l+w)$, instead of the sample area lw which applies only if the sample is far away from the window. The exposure time must then be multiplied by a correction factor R which is obtained from the ratio of the areas $R=(1/2d)[lw/(l+w)]$. For our last sample (3) with a gap of 75 μm, $R\sim30$. Experimentally, we did observe exposure times of about 15 to 30 L to reach saturation coverage in contrast to only a few Langmuirs for unrestricted sample geometries, as determined by other workers. The monitoring of the exposure time was useful for a relative comparison between runs rather than an absolute determination of the gap.

The two main difficulties encountered in this experiment were the alignment of the sample and the signal-to-noise ratio. The alignment, as described above, was satisfactory. Our optical method of monitoring the SEW throughput versus gap did allow good control over the relative position of the sample with respect to the window. However, one serious difficulty with the experimental geometry which we discovered was that low-frequency vibrations of the sample with respect to the window modulated the gap and gave rise to a very poor signal-to-noise ratio. To eliminate the vibrations it was necessary to tilt the sample so as to touch the window with one crystal edge while maintaining a constant gap at the center of the crystal where the SEW's were propagating. Unfortunately this experimental arrangement eliminated the possibility of temperature-dependent measurements.

D. SEW results

We found that the most reliable way of obtaining the transmission data was to record both ΔI and I as a function of H_2 exposure for a given laser frequency. By repeating the run for different laser frequencies, one could then obtain a curve of $\Delta I/I$ versus frequency. A typical example of the raw data obtained in this way is given in Fig. 7, where the transmission signal is plotted for saturation coverage ($\Theta=2$) at two frequencies: 1045 cm^{-1} at the peak of the absorption and 1075 cm^{-1} above the absorption line. The small dip for the 1075-cm^{-1} data at intermediate coverages

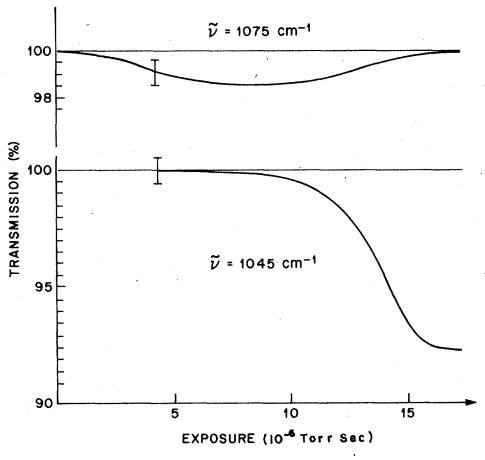

FIG. 7. Sketch of the raw data obtained for two typical runs. The top is for 1075 cm^{-1} [R(14)] where the line passes through. The bottom is for 1045 cm^{-1} [P(22)] where the line peaks at saturation coverage.

TABLE I. Summary of the raw and corrected $(\Delta I/I)_{\text{saturation}}$ obtained for different laser frequencies.

Laser line (transition index)	Frequency (cm^{-1})	Measured throughput I/I_0	Gap estimate from throughput of Fig. 4(b) (μm)	Correction factor (1/sensitivity)	$\Delta I/I$ (Raw) (%)	$\Delta I/I$ (Corrected) (%)
P(22)	1045	0.88	78	1	8	8
P(12)	1054	0.90	80	1	3.6	3.6
P(28)	1039.5	0.75	70	1	4.2	4.2
P(28)	1039.5	0.81	74	1	4.6	4.6
P(18)	1049	1.50	120	2	2.8	5.6
P(18)	1049	1.40	115	1.75	3.4	6.0
P(12)	1054	1.40	115	1.75	1.9	3.3
P(20)	1047	0.20	30	2	4.1	8.2
R(14)	1075	0.70	65	1	1.8 → 0	1.8 → 0
R(22)	978	0.56	55	1.1	0	0
R(10)	1072	0.25	40	1.25	1.5 → 0	1.9 → 0
R(14)	1075	0.80	74	1	1.15 → 0	1.15 → 0

is due to the vibrational absorption line moving from a higher frequency (1250 cm^{-1} for $\Theta = 0.5$) to a lower frequency (1045 cm^{-1} for $\Theta = 2$).[33]

The lower trace shows that the saturation coverage configuration starts after about 8 L (uncorrected for gauge sensitivity). Using the correction factor $R \sim 30$ derived in the previous section for a 75-μm gap, and correcting for gauge sensitivity, the saturation configuration is estimated to start around 0.5 L and to end by 1 L exposure. (For these two runs, the gap was estimated to be ~75 μm from the throughput ratio.) For a gap of 75 μm, Fig. 4(b) shows that the effective sensitivity to the adsorbate is 1. For other values of the gap, however, the recorded values of $(\Delta I/I)$ must be corrected by dividing them by the sensitivity given in Fig. 4(b). Table I summarizes the results.

A second way of obtaining the transmission data is to sweep frequency and record the SEW transmission both before and after hydrogen exposure. The data obtained this way have a larger error bar because of laser drifts. A particularly good run is shown in Fig. 8, where the normalized transmission is plotted versus frequency.

Combining all the data, we obtain the percent absorption versus frequency curve shown in Fig. 9. The data can be fit with a Lorentzian (solid line) peaked at 1046 cm^{-1} and with a full width at half maximum (FWHM) of 14 cm^{-1} or with a Gaussian (dashed line) with $2\sigma = 11$ cm^{-1}. The integrated line strength is $\int \alpha(\tilde{\nu}) d\tilde{\nu} = 0.93$ cm^{-2}.

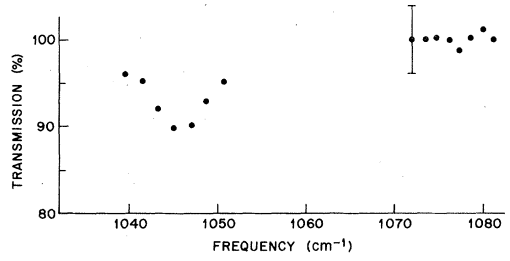

FIG. 8. Transmission of SEW's on an H-covered W(100) surface ($\Theta = 2$) normalized by that of a bare W(100) surface. The gap is approximately 75 μm.

III. COMPARISON OF SEW AND EELS RESULTS

A. Effective charge of the ν_1 vibrational mode

So far, we have seen that for saturation coverage of H on W(100) the absorption line measured

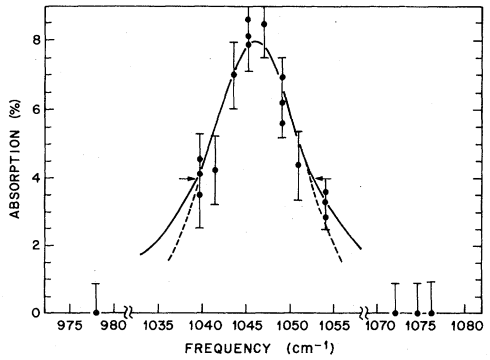

FIG. 9. The hydrogen-induced SEW absorptivity on W(100) at saturation coverage versus frequency. $\Delta I/I$ is given in percent and the frequency in cm^{-1}. Note the discontinuous frequency scale. The solid line is the Lorentzian fit and the dashed line the Gaussian fit described in the text.

by SEW spectroscopy occurs at the same peak frequency (approximately 130 meV) as measured by EELS.[12-14,33] Let us now compare the line strength as determined by the two techniques. The integrated line strength can be related to the effective charge of the oscillating dipole for the ν_1 mode by adapting the optical sum rule to the SEW transmission data.

1. The optical sum rule for SEW's

The absorption coefficient of a plane wave through a homogeneous medium is related to the number density of absorbing centers by the optical sum rule[34]

$$\int_{\substack{\text{absorption}\\ \text{band}}} \alpha(\tilde{\nu})d\tilde{\nu} = \pi\left(\frac{Ne^{*2}}{M^{*}c^{2}}\right)\left|\frac{E_{\text{eff}}}{E}\right|^{2}\epsilon^{-1/2}, \quad (17)$$

where $\tilde{\nu}$ is the frequency in cm^{-1}, N is the concentration of absorbing centers (in cm^{-3}), e^{*} and M^{*} are the effective charge and mass of the normal mode, and ϵ is the dielectric constant of the host medium averaged over the frequency region of interest. E_{eff} is the effective field at the absorbing center and $\boldsymbol{E}$ is the applied field. In the case of SEW absorption by centers located on a metal surface, this relation can be modified to treat this inhomogeneous problem.

In the 10-μm region, almost all of the energy (99.9%) contained in SEW's is located outside the metal on the vacuum side where $\epsilon = 1$. In this region and close to the metal (~10 Å), where the adsorbate is located, SEW's resemble plane waves since the real part of their propagation wave vector $\text{Re}(k_x) \cong \omega/c$. If SEW's could exist with no metal substrate, then $|E_{\text{eff}}/E|^{2} \sim 1$ in Eq. (17); however, the presence of the metal will have the effect of modifying the dynamic dipole moment "seen" by the electromagnetic field. In the long-wavelength limit (static limit), the metal produces an image of the oscillating dipole and the electric field interacts coherently with both moments. For this mode the dipole and its image add in phase to produce an oscillating dipole of twice the size of the original. Equivalently, the oscillating dipole can be taken as unchanged but then the effective field must be doubled to account for the metal contribution. This enhancement can be included in Eq. (17) by setting $E_{\text{eff}}/E = 2$. This approximation ignores any adsorbate-adsorbate interaction or any local-field effects. Such corrections can be introduced through additional changes in $|E_{\text{eff}}/E|^{2}$ in Eq. (17).

One can compare the density of absorbing centers N to a coverage by recalling that the SEW energy is located above the metal, and decays exponentially into the vacuum with a characteristic decay length δ, which depends entirely on the metal-optical constants.[23] Hence,

$$N = N_s/\delta\ , \quad (18)$$

where N_s is the coverage in centers/cm^2. For SEW spectroscopy, the absorption induced by the adsorbate is defined as

$$\alpha_a = (1/l)\ln(1 - \Delta I/I)\ , \quad (19)$$

where l is the length over which the SEW propagates along the surface, and ΔI is the change in transmitted intensity I, due to the presence of the adsorbate. For α_a defined above, Eq. (17) becomes

$$\int_{\substack{\text{absorption}\\ \text{band}}} \alpha_a(\tilde{\nu})d\tilde{\nu} = (4\pi\delta^{-1})\left(\frac{e^{*2}}{M^{*}c^{2}}\right)N_s\ . \quad (20)$$

The left-hand side of Eq. (20) can be measured directly from the $\alpha(\tilde{\nu})$ curve; the first factor in parentheses on the right-hand side of Eq. (20) depends only on the metal-optical constants, while the second factor in parentheses depends only on the vibrational-mode parameters. As expected, the strength of the absorption is proportional to the coverage N_s. One must keep in mind that the factor 4 comes from the long-wavelength approximation where the image dipole has the same strength as the real dipole.

2. Test of the sum rule

In order to test Eq. (20), a few monolayers of an absorbing molecule, potassium perrhenate ($KReO_4$), were evaporated on a gold film. The results have been reported without the image-charge correction factor.[32] The corrected results are summarized in Table II. Column 2 gives the experimentally determined $KReO_4$ coverage which was determined in two ways: (1) geometrically by measuring the mass of $KReO_4$ evaporated and the solid angle subtended by the metal film and (2) analytically, by neutron activation of the Re atoms. Both techniques agree to within 50% with the former, consistently giving a lower value. From the structure of solid $KReO_4$ we estimate the effective volume of one molecule of $KReO_4$ to be 102 Å.[35] Using the billiard ball model, we estimate the surface density for one monolayer to be $N_s = 4\times10^{14}$ cm^{-2}.

The third column gives the experimentally measured line strength. The last column shows the theoretical estimate of the line strength for the value e^{*} determined by Eq. (20). The other parameters required are N_s (column 2), $M^{*} = 14.5$ amu (Ref. 36), and $\delta = 64$ μm.[37] The last column shows that if $e^{*}/e = 0.67$, then the experimental results

TABLE II. Test of the surface-wave-oscillator-strength sum rule—a summary of the data observed for $KReO_4$-coated gold films.

Run number	Experimentally determined coverage (cm^{-2})	Experimentally measured integrated absorption (cm^{-2})	Theoretical estimate of the line strength using Eq. (5) with $e^*/e=0.67$ (cm^{-2})
1	3.3×10^{15}	33	31
2	2.3×10^{15}	20	21
3	1.8×10^{15}	15	17
4	2.3×10^{15}	18	21

in column 3 are reproduced. In another ir study of ReO_4^- molecules in KI, a value $e^*/e\approx1$ was obtained.[38] The difference between this value and that found in the last column of Table II probably can be ascribed to local-field effects. Since the measured coverages in Table II are much larger than a single monolayer, bulk local-field corrections cannot be ignored.

Because of the local-field correction uncertainty an additional independent check of the sum rule [Eq. (20)], using published data, is given in Appendix A, where it is shown that the measured parameters of the stretch mode of chemisorbed CO on Pt(111) obtained with EELS can be used together with the sum rule to confirm the experimental results obtained by RA spectroscopy.

3. *H on W(100)*

For H on W(100), the coverage N_s, the effective mass M^*, and the SEW decay height δ, can be accurately determined so that an estimate of e^* can be made. From emissivity measurements,[31] one gets $\omega_p\tau=140$ at room temperature in the 10-μm region. Low-temperature reflectivity data[39] yield $\omega_p=8.9\times10^{15}$ rad/sec so that $\delta=(c\omega_p/2\omega^2)\cong34$ μm at 1046 cm^{-1}. With $M^*=1$ amu, $N_s=2\times10^{15}$ H/cm^2, and from the measured integrated absorption $\int\alpha d\nu=0.93$ cm^{-2}, Eq. (20) yields $e^*/e=0.03\pm0.01$ (SEW). Inherent in this estimate is the image-charge enhancement and the neglect of any local-field effects. This value is in reasonable agreement with the estimate obtained from EELS data,[40] which is $e^*/e=0.05$ (EELS). Although the error was not reported for the estimate from the EELS data, we estimate it to be ±0.01 (see Appendix B). The fact that the SEW derived e^* lies below the EELS derived e^* will be discussed in the next section.

B. Spectral shape of the ν_1 vibrational mode

The major difference between the SEW and EELS measurements is in the spectral linewidths $\Delta_{SEW}=14$ cm^{-1} while the $\Delta_{EELS}=118$ cm^{-1}. It is also known that the EELS and RA techniques measure the same linewidth for the internal mode (C–O stretch) of CO on Pt(111).[41,42] Either SEW spectroscopy is somehow different from RA spectroscopy, which seems unreasonable, or the ν_1 for H on W(100) does not have a simple spectral shape. The different resolving powers of SEW and EELS then could provide different averages of the resultant spectral shape. In general, the dynamic coupling of a vibrational mode to the lattice would be expected to be larger for a metal-adsorbate vibrational mode than for an internal mode of an adsorbed molecule. Since H does induce a large static rearrangement of the surface W atoms as the coverage is increased, a large dynamic coupling between the hydrogen and the phonons of tungsten is to be expected.

1. *One-phonon sidebands*

For low H coverage the sideband spectrum can be calculated by considering an anharmonic coupling term of the form Q^2q, where the ν_1 mode coordinate is denoted by Q and the rest of the lattice normal modes by $\{q_l\}$.[43,44] This anharmonic coupling of the ν_1 mode to the surface phonons changes the spectral shape of the absorption band from a single band associated with the excitation of the ν_1 mode to a line plus two sidebands; the sidebands are associated with two vibrational-mode transitions.[45] The sideband processes can be seen as follows: A ν_1 mode quantum is virtually excited by an absorbed photon. This state decays into a final state in which one ν_1 mode quantum is created and one surface-phonon-mode quantum is either created or destroyed. In this framework, any peak in the density of surface phonons would appear as peaks in the sideband spectrum.

The lowest-order coupling between the hydrogen vibration and surface phonons gives an absorption coefficient which can be written as[46]

$$\frac{\alpha(\omega)}{\omega} \sim \delta(\omega-\Omega)+\sum_l |(X,l)|^2 \frac{\hbar[n(\omega_l)+1]}{2\omega_l}\left(C+\frac{B}{2M^*\Omega\omega_l}\right)^2 \delta(\omega-\Omega-\omega_l)$$
$$+\sum_l |(X,l)|^2 \frac{\hbar n(\omega_l)}{2\omega_l}\left(C-\frac{B}{2M^*\Omega\omega_l}\right)^2 \delta(\omega-\Omega+\omega_l)\,, \tag{21}$$

where the first term represents the zero-surface-phonon ν_1 mode, the second term after the plus, the $n=+1$-surface-phonon sideband, and the third term, in the last line, the $n=-1$ sideband. In Eq. (21), ω is the radiation frequency, Ω is the frequency of the uncoupled H-W_2 vibrational mode with effective mass M^*, $|(X,l)|^2$ is a coefficient describing the projection of the H-W_2 configurational coordinate onto the surface-phonon coordinate q_l, with frequency ω_l, C is the coefficient for second-order dipole coupling, and B the coefficient for anharmonic coupling. Equation (21) is adequate for calculating the relative intensities of the sidebands with respect to the zero-phonon line at fixed temperature. Although a temperature-dependent measurement has not yet been carried out on the ν_1 mode, it should be noted that the complete absorption spectrum associated with the mode is expected to be temperature independent at least for an anharmonic system with a linear dipole moment. For this model, raising the temperature increases the absorption in the sidebands at the expense of the absorption in the zero-surface-phonon line.

The description which we have given so far applies only to an isolated H on the W surface. For a monolayer coverage of H on W(100) the phonon momentum in the plane of the surface remains a good quantum number so Ω becomes $\Omega(\vec{K})$. The zero-phonon line occurs at $\Omega(0)$ due to the usual $\vec{K}=0$ selection rule for light. The one-phonon sidebands occur at

$$\omega=\Omega(\vec{K})\pm\omega_l(\vec{\kappa})\,. \tag{22}$$

Since the wave-vector selection rule is now $\vec{K}=-\vec{\kappa}_\parallel$ with $\vec{\kappa}_\perp$ arbitrary, Eq. (22) becomes

$$\omega=\Omega(-\vec{\kappa}_\parallel)\pm\omega_l(\vec{\kappa}_\parallel,\vec{\kappa}_\perp)\,. \tag{23}$$

One possible change in the sideband spectrum on going to full coverage could be due to the effect of the dispersion of $\Omega(\vec{K})$, which must, in some complicated way involving $\vec{K}=-\vec{\kappa}_\parallel$, be folded into the phonon spectrum. If the dispersion in $\Omega(\vec{K})$ is much less than the Debye frequency of the W surface then there should be no change in the spectrum in going from the dilute limit to full coverage.

2. *Experimental evidence for surface sidebands*

We assume that the sharp spectral feature with width ($\Delta=14$ cm^{-1}) observed by SEW spectroscopy is the zero-phonon line and the broad spectral feature with width ($\Delta=118$ cm^{-1}) observed by EELS spectroscopy is the complete absorption band of the ν_1 mode, but at low resolution. We also assume that the SEW spectroscopy with EELS sensitivity would give the same absorption spectrum as EELS spectroscopy with SEW resolution. We show below that these two assumptions are consistent with the experimental data.

In Fig. 10, both the EELS and SEW data are combined to extract the sideband spectrum. The procedure is as follows: First, the resolved (SEW) zero-phonon line is convoluted with the EELS resolution to obtain the dotted curve (C); next, curve (C) is subtracted from the EELS spectrum to obtain the sum and difference bands labeled D_+ and D_-. The resolved spectral information is represented by the solid curve (ir) and the constructed sideband curves D_+ and D_-. To check the consistency of this construction, we compare the relative intensity of the two sidebands with that predicted by Eq. (21).

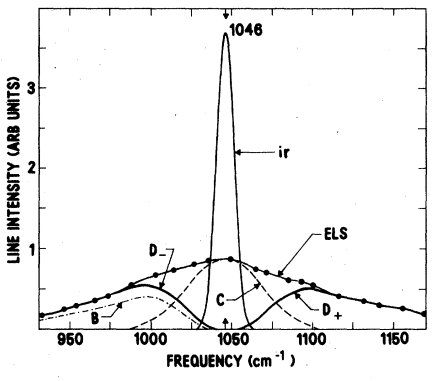

FIG. 10. The ν_1 vibrational band as observed by SEW and EELS. (ir) is the measured absorption line and C the same line convoluted with the EELS resolution function. The lines D_+ and D_- are obtained by subtracting the convoluted ir line C from the EELS raw data. Line B is the prediction of Eq. (21) using D_+ in order to determine the $\Delta n=-1$ sideband in the limits of anharmonic coupling or second-order dipole-moment coupling.

The relative strength of D_+ to D_- is calculated as a function of the coupling-constant ratio $R \equiv B/2M^*\Omega^2 C$. For $R=0$, i.e., pure second-order dipole-moment coupling, the intensity ratio of the $\Delta n=-1$ sideband to the $\Delta n=+1$ sideband is

$$\frac{\alpha(\Delta n=-1)}{\alpha(\Delta n=+1)} = \frac{n(\omega_t)}{n(\omega_t)+1} \quad . \tag{24}$$

For $T=300$ K, curve B is obtained in Fig. 10. As R is increased so that a mixture of the two types of coupling is allowed, the ratio decreases for each ω_t until the $\Delta n=1$ sideband is almost completely extinguished, due to the interference between the two types of coupling. As R increases still farther, the calculated $\Delta n=-1$ sideband grows relative to the $\Delta n=+1$ sideband. Finally, for a purely anharmonic coupling ($R \to \infty$ as $C \to 0$), the ratio is again given by Eq. (24). At this stage, it is not possible to distinguish experimentally between the two mechanisms but the data shows that, within this model, one mechanism must dominate. A comparison of the experimental error bars for the SEW data in Fig. 9 with the strength of the sidebands in Fig. 10 shows that the sidebands are too weak to be seen with the present SEW sensitivity.[47]

An additional check of the consistency of the two sets of data with the anharmonic-coupling model can be made by means of the optical sum rule. From Eq. (20), the area under the absorption curve is proportional to the square of the effective charge e^*. Since the SEW technique is only sensitive enough to see the sharp zero-phonon line, then the effective charge as measured by this probe should be smaller than the effective charge as measured by EELS, which measures the total band. From Fig. 10, the ratio of the zero-phonon line (ZPL) area to the total absorption band area is $\sim \frac{1}{2}$. By Eq. (20), the ratio of the effective charge associated with the ZPL to that associated with the entire band is

$$\frac{(e^*)_{\mathrm{ZPL}}}{(e^*)_{\mathrm{band}}} \approx \frac{1}{\sqrt{2}} \quad . \tag{25}$$

Although the error bars on the effective charges measured by the SEW and EELS measurements are large, it is satisfying to find that the ratio

$$\frac{(e^*)_{\mathrm{SEW}}}{(e^*)_{\mathrm{EELS}}} \sim 0.6$$

is in reasonable agreement with Eq. (25).

IV. CONCLUSIONS

For the first time a high-resolution ir spectroscopic technique has been used to measure the vibrational spectrum of an adsorbate-metal bond at a single crystal surface under UHV conditions. The surface-electromagnetic-wave (SEW) spectroscopic technique provides an order-of-magnitude increase in contrast over that derived from conventional reflection-absorption spectroscopy. Using a line-tunable CO_2 laser as a source, we have been able to resolve a sharp absorption band associated with the symmetric stretching mode ν_1 of H on W(100). Although our limited signal to noise and restricted frequency range have made it impossible to confirm that phonon sidebands also occur, such sidebands are required to explain the broad band measured for the ν_1 mode with electron-energy-loss spectroscopy (EELS). The two apparently contradictory results can be made consistent by invoking a model where the ν_1 mode is strongly coupled to W bulk phonons. The SEW technique, which has high resolution but low sensitivity, probes only the zero-phonon line while the EELS technique, which has high sensitivity but lacks energy resolution, probes the zero-phonon line plus the sum and difference sidebands.

This dynamical-coupling model also provides a natural explanation of the sharper transition observed in EELS at low H coverage. The experimental evidence is that the reconstructed surface of tungsten has a W–H–W bond angle of 89° while the high coverage β_1 phase has a bond angle of 108°.[33] A simple geometric argument would suggest that the coupling between the surface motion and the perpendicular vibration will decrease as the bond angle decreases. Weak static coupling implies weak dynamic coupling, and most of the intensity would remain in the zero-phonon transition.

Temperature-dependent measurements of the ν_1 band with EELS should provide a straightforward test of the linear-phonon-coupling model: At low temperatures, the $\Delta n=-1$ sideband is suppressed, while at high temperatures ($T > \Theta_D$) the $n=-1$ sideband is larger than the $n=+1$ sideband if the dominant mechanism is due to anharmonic coupling.

Another test of this model would consist of a high-resolution study of the ν_1 mode of deuterium on W(100). For anharmonic coupling the integrated area in the sidebands relative to the main band should only be half as large as for the hydrogen case, while it should be independent of M^* for second-order dipole coupling.

The linear-coupling model described by Eq. (21) does not account for the SEW measured width of the ZPL. If quadratic and higher-order coupling to surface and bulk phonons is included, then the ZPL has a width and center frequency which change with temperature.[44,45]

Both decomposition and scattering processes would broaden the ZPL by limiting the lifetime of the excited vibrational state. In the decomposition process the ZPL would decay into a number of phonons. At low temperatures this process would produce a constant width while at high temperatures an n-phonon decay would produce a width which varies like $T^{(n-1)}$. The scattering processes associated with quadratic coupling would produce a T^6 dependence to ZPL width at low temperatures and a T^2 dependence at high temperatures. A general conclusion which emerges from this work is that high-resolution spectroscopy of metal-adsorbate vibrational modes can yield a wealth of information on the details of the dynamical coupling of adsorbed molecules to the metal-surface atoms.

ACKNOWLEDGMENTS

R. H. Silsbee has been particularly helpful at all stages of this research. We would also like to thank T. W. Capehart, G. W. Graham, and Z. Schlesinger for many useful discussions, and B. Addis for orienting, cutting, and polishing the W crystals. This work was supported by the National Science Foundation through a grant to the Cornell Materials Science Center (No. DMR-76-81083A02).

APPENDIX A: TEST OF THE SUM RULE FOR CO ON Pt(111)

The validity of the sum rule given in Eq. (20) can be tested for a particular system such as CO on Pt(111), where both EELS and ir reflection data exist. From EELS experiments, we get the following parameters: $N_s = 7.2\times10^{14}$ cm^{-2}, $\Delta = 12$ cm^{-1}, $M^* = 6.9$ amu, $e^*/e = 0.79$.[40] In addition, from extrapolation of 10-μm data, we estimate $l_{opt} \cong 9\times10^{-2}$ cm and $\delta = 7\times10^{-4}$ cm at 5 μm so that $l_{opt}/\delta \cong 1.3\times10^2$. We now have all the parameters necessary to calculate δ from the sum rule given in Eq. (20):

$$\alpha_{max} l_{opt} = \frac{4\pi}{\Delta}\frac{l_{opt}}{\delta}\left(\frac{e^*}{M^* c^2}\right) N_s = 1.36 ,$$

so that

$$\left(\frac{\Delta I}{I}\right)_{peak} = 1 - e^{-\alpha_{max} l_{opt}} = 74\% .$$

Next, we use Eq. (14) to predict $\Delta R/R$ from $\Delta I/I$. For one reflection at $\theta = 85°$,

$$\left(\frac{\Delta R}{R}\right)_{peak} \simeq \left(\frac{1}{2\omega_p \tau}\right)\left(\frac{\sin^2\theta}{\cos\theta}\right)\left(\frac{\Delta I}{I}\right)_{peak} \simeq 7\% - 3\% ,$$

depending on which value for $\omega_p\tau$ is chosen (in the range $\omega_p\tau = 60$ to $\omega_p\tau = 140$). Thus, by means of the sum rule and of Eq. (14), we use the EELS determined e^* to predict that $(\Delta R/R)_{peak} \cong 5\%$. Experimentally, for one reflection at $\theta = 85°$, RA spectroscopy does measure $(\Delta R/R)_{peak} \sim 5\%$ (Ref. 41).

The same set of equations allows us to determine what the peak absorption $\Delta R/R$ would be for the H/W(100) system. Assuming one reflection at 85° incidence, we estimate that, if $\Delta I/I = 8\%$ as measured, then $\Delta R/R \sim 0.3\%$.

APPENDIX B: ESTIMATE OF THE EELS ERROR BAR FOR THE e^* VALUE

To calculate e^* from the EELS spectra, one requires the knowledge of the optical constants of the metal at the frequencies involved, the acceptance angle of the spectrometer, the accurate determination of the specular reflection angle, and of the determination of the true primary energy of the electron beam. Once these parameters are determined, the relative determination of e^* for different adsorbates on W(100) can be accurate. For example, Ibach reports $e^*/e = 0.052$ for the system H on W(100) and $e^*/e = 0.055$ for the system D on W(100).[40] Since these two results should be identical, the relative error can be seen to be as low as 6%. The absolute determination, however, may have a systematic error. For instance, the error in the determination of the primary energy yields an uncertainty of 9% in the value of e^*, while the error in the optical constants and angle determination could add another 10%. On the whole, we can assign a rough error bar to the EELS experimental estimate of e^*, namely 25%, so that $(e^*/e)_{EELS} \cong 0.05 \pm 0.01$.

---

*Present address: Bell Laboratories, Murray Hill, N.J. 07974.

[1]A spectral resolution of 1 to 5 cm^{-1} (i.e., less than 1 meV) is typical, as exemplified in the reviews of L. H. Little, in *Chemisorption and Reactions on Metallic Films*, edited by J. R. Anderson (Academic, New York, 1971), p. 489, Vol. 1 and M. L. Hair, *Infrared Spectroscopy in Surface Chemistry* (Dekker, New York, 1967).

[2]S. A. Francis and A. H. Ellison, J. Opt. Soc. Am. 49, 131 (1959).

[3]J. Pritchard and M. L. Sims, Trans. Faraday Soc. 66, 427 (1970).

[4]H. G. Tompkins and R. G. Greenler, Surf. Sci. 28, 194 (1971).

[5]J. T. Yates and D. A. King, Surf. Sci. 30, 601 (1972).
[6]J. Pritchard, T. Catterick, and R. K. Gupta, Surf. Sci. 53, 1 (1975).
[7]A. Crossley and D. A. King, Surf. Sci. 68, 528 (1977).
[8]M. G. Wells, W. W. Cant, and R. G. Greenler, Surf. Sci. 67, 541 (1977).
[9]J. D. E. McIntyre, in *Optical Properties of Solids, New Developments*, edited by B. O. Seraphin (North-Holland, Amsterdam, Oxford, and New York, 1976), Chap. 11.
[10]H. Ibach, Phys. Rev. Lett. 27, 253 (1971).
[11]S. Anderson, Solid State Commun. 21, 75 (1977).
[12]A. Adnot and J.-D. Carette, Phys. Rev. Lett. 39, 209 (1977).
[13]H. Froitzheim, H. Ibach, and S. Lehwald, Phys. Rev. Lett. 36, 1549 (1976).
[14]W. Ho, R. F. Willis, and E. W. Plummer, Phys. Rev. Lett. 40, 1463 (1978).
[15]I. Batra, K. Hermann, A. M. Bradshaw, and K. Horn, Phys. Rev. B 20, 801 (1979).
[16]H. Pfnür, D. Menzel, F. M. Hoffman, A. Orbega, and A. M. Bradshaw, Surf. Sci. 93, 431 (1980).
[17]K. Yonehara and L. D. Schmidt, Surf. Sci. 25, 238 (1971).
[18]M. K. Debe and D. A. King, Surf. Sci. 81, 193 (1979); Phys. Rev. Lett. 39, 708 (1977); D. A. King and G. Thomas, Surf. Sci. 92, 201 (1980).
[19]T. E. Felter, R.A. Barker, and P. J. Estrup, Phys. Rev. Lett. 38, 1138 (1977); R. A. Barker and P. J. Estrup, *ibid.* 41, 1307 (1978).
[20]I. Stensgaard, L. C. Feldman, and P. J. Silverman, Phys. Rev. Lett. 42, 247 (1979).
[21]K. Bhasin, D. Bryan, R. W. Alexander, and R. J. Bell, J. Chem. Phys. 64, 5019 (1976); D. L. Begley, D. A. Bryan, R. W. Alexander, R. J. Bell, and C. A. Caben, Surf. Sci. 60, 99 (1976).
[22]G. N. Zhizhin, M. A. Moskaleva, E. V. Shomina, and V. A. Yakovlev, Zh. Eksp. Teor. Fiz. Pis'ma Red. 24, 221 (1976) [JETP Lett. 24, 196 (1976)].
[23]R. W. Alexander, R. J. Bell, and C. A. Ward, in *Electromagnetic Surface Modes*, edited by A. D. Boardman (Wiley, New York, 1980).
[24]Y. J. Chabal and A. J. Sievers, Phys. Rev. Lett. 44, 944 (1980).
[25]J. Schoenwald, E. Burstein, and J. M. Nelson, Solid State Commun. 12, 185 (1973).
[26]Z. Schlesinger and A. J. Sievers, Surf. Sci. Lett. 102, L29 (1981).
[27]R. G. Greenler, J. Chem. Phys. 50, 1963 (1969); J. Vac. Sci. Technol. 12, 1410 (1975).
[28]T. C. Fry, J. Opt. Soc. Am. 22, 307 (1932).
[29]Y. J. Chabal and A. J. Sievers, Appl. Phys. Lett. 32, 90 (1978).
[30]The differentially pumped double O-ring seal developed by Pritchard and Hollins appears to be a better design. P. Hollins and J. Pritchard, J. Vac. Sci. Technol. 17, 665 (1980).
[31]L. A. Wojcik, A. J. Sievers, G. W. Graham, and T. N. Rhodin, J. Opt. Soc. Am. 70, 443 (1980).
[32]Y. J. Chabal and A. J. Sievers, J. Vac. Sci. Technol. 15, 638 (1978).
[33]M. R. Barnes and R. F. Willis, Phys. Rev. Lett. 41, 1729 (1978); R. F. Willis, Surf. Sci. 89, 457 (1979).
[34]D. J. Dexter, Phys. Rev. 101, 48 (1956); W. T. Doyle, *ibid.* 111, 1072 (1958); P. E. Dawber and R. J. Elliot, Proc. Phys. Soc. London 81, 453 (1963).
[35]J. C. Morrow, Acta Crystallogr. 13, 443 (1960).
[36]G. Herzberg, *Molecular Spectra and Molecular Structure: II. IR and Raman Spectra of Polyatomic Molecules* (Van Nostrand Reinhold, New York, 1945), p. 182.
[37]H. E. Bennett and J. M. Bennett, *Proceedings of the International Colloquium on Optical Properties, Paris, 1965*, edited by F. Abeles (North-Holland, Amsterdam, 1966), p. 175.
[38]A. R. Chraplyvy and A. J. Sievers, Opt. Lett. 3, 112 (1978).
[39]J. H. Weaver, C. G. Olson, and D. W. Lynch, Phys. Rev. B 12, 1293 (1975).
[40]From: H. Ibach, Surf. Sci. 66, 56 (1977). However, due to a missing factor of 2 in Eq. (25) of this reference, all values of e^* are too low by a factor of $\sqrt{2}$. See, A. M. Braro, H. Ibach, and H. D. Bruchmann, Surf. Sci. 88, 384 (1979).
[41]R. A. Shigeishi and D. A. King, Surf. Sci. 58, 379 (1976); K. Horn and J. Pritchard, J. Phys. (Paris) 38, C4-164 (1977); H.-J. Krebs and L. Lüth, Appl. Phys. 14, 337 (1977).
[42]H. Froitzheim, H. Hopster, H. Ibach, and S. Lehwald, Appl. Phys. 13, 147 (1977).
[43]H. Frauenfelder, *The Mössbauer Effect* (Benjamin, New York, 1962).
[44]R. H. Silsbee, Phys. Rev. 128, 1726 (1962).
[45]A. S. Barker, Jr. and A. J. Sievers, Rev. Mod. Phys. 47, S-2 (1975).
[46]M. V. Klein, *Physics of Color Centers*, edited by W. B. Fowler (Academic, New York, 1968), p. 518.
[47]We note that, since this work was first published in Ref. 13, Ibach and co-workers have observed two weak peaks distributed symmetrically around the Ni-CO vibrational loss peak which could be attributed to the same mechanism. B. N. J. Persson and H. Ibach, Surf. Sci. 99, 283 (1980).